Rapid Exciton Transport and Structural Defects in Individual Porphyrinic Metal Organic Framework Microcrystals

Sajia Afrin [1,2], Xiaozhou Yang [3], Amanda J. Morris* [3], Erik M. Grumstrup* [1,2].

AUTHOR ADDRESS 1. Department of Chemistry and Biochemistry, Montana State University, Bozeman, Montana 59717 United States; 2. Montana Materials Science Program, Montana State University, Bozeman, Montana 59717 United States; 3. Department of Chemistry, Virginia Tech, Blacksburg, Virginia 24061, United States.

KEYWORDS: Pump-Probe Microscopy, Exciton Transport, Ultrafast Dynamics, Photoluminescence Microscopy.

ABSTRACT: To date, spectroscopic characterization of porphyrin-based metal organic frameworks (MOFs) has relied almost exclusively on ensemble techniques, which provide only structurally-averaged insight into the functional properties of these promising photochemical platforms. This work employs time-resolved pump-probe microscopy to probe ultrafast dynamics in individual PCN-222 MOF single crystals. The simultaneous high spatial and temporal resolution of the technique enables the correlation of spectroscopic observables to both inter- and intra- crystal structural heterogeneity. The pump-probe measurements show that significant differences in excited state lifetime exist between individual PCN-222 crystals of an ensemble. On a single PCN-222 crystal, differences in excited state lifetime and photoluminescence quantum yield are found to correlate to microscale structural defects introduced at crystallization. Pump probe microscopy also enables direct measurement of excited state transport. Imaging of exciton transport on individual MOF crystals reveals rapid, but sub-diffusive exciton transport which slows on the 10s of ps timescale. Time-averaged exciton diffusion coefficients over the first 200 ps span a range of 0.27 to 1.0 cm^2/s, indicating that excited states are rapidly transported through the porphyrin network of PCN-222 before being trapped. Together, these single-particle resolved measurements provide important new insight into the role played by structural defects on the photochemical functionality of porphyrin-based MOFs.

Metal-Organic Frameworks (MOFs), with their characteristic high porosity[1], large specific surface area[2], facile chemical tunability[3], and range of topological structures[4], are the subject of diverse fundamental and practical interest.[5] For light harvesting and photochemical applications, the highly-ordered, dense chromophore packing of MOFs can be leveraged to achieve favorable photophysical properties, including large extinction coefficients and efficient energy transfer.[6-8] Characterization of such properties often leverages steady state and time-resolved photoluminescence (PL) and absorption spectroscopies, techniques that probe a large ensemble of MOF particles.

While the current understanding of MOF excited state dynamics is largely derived from ensemble spectroscopic studies, recent work suggests that single-particle probes might reveal previously hidden links between structure and photophysical function.[9, 10] For example, linkers and node site vacancies, which vary between individual particles, are increasingly recognized as important determiners of MOF functionality.[11] Many MOFs also exhibit long-range, extended electronic structure that transcends the "zeroth-order" molecular (ensemble) picture to enable long-range (~50-100 nm) energy transport[7, 8, 12, 13, 14] and band-like charge transport.[15] The implication of such long range electronic coupling is that inter- and intra-particle differences in electronic structure, caused by local variation in morphology, may strongly influence MOF functional properties.[9, 10, 16] Because ensemble probes only provide a structure-averaged observable, they may obscure important variables that are significant determiners of photophysical functionality.

Here we utilize time-resolved pump-probe microscopy (PPM) and PL microscopy to investigate individual PCN-222 (free base) MOF microrods. With its prototypical porphyrin network and large aspect ratio crystals, PCN-222 is an ideal candidate for single particle studies.[8, 17] The microscopy measurements reveal two key insights about excited state evolution in PCN-222. First, by directly measuring spatial evolution of the Q-band photoinduced absorption, we find exceptionally rapid, but sub-diffusive exciton transport through the porphyrin network. The sub-diffusive transport suggests that excitons are rapidly trapped, within the first ~50 ps after photoexcitation, due to structural or chemical defects in the PCN-222 microrods. Second, we find significant spatial variation of excited state relaxation dynamics both within and between individual PCN-222 microrods. Spatial variation in excited state lifetime and photoluminescence quantum yield is extreme in regions where the microrods are bent. These bent regions are believed to result from defects that accumulate during growth, resulting in a reoriented preferential growth direction. While specific to PCN-222, these results highlight the broader importance of crystal

defects in determining the photophysical and photochemical behavior of light-active MOFs.

PCN-222 microrods were prepared by suspending $ZrOCl_2 \cdot 8H_2O$, TCPP, and DFA in DMF in a scintillation vial and placing the suspension in an oven held at 120°C for 18 hours. The resultant violet powder was centrifuged and washed with DMF and acetone. The obtained microrod powder was dried under vacuum at 60 °C overnight.[18] To prepare samples for microscopy studies, The PCN-222 microrods were dispersed in ethanol, spin-coated onto a glass substrate, and heated at 200°C for 10 minutes to ensure complete solvent evaporation.

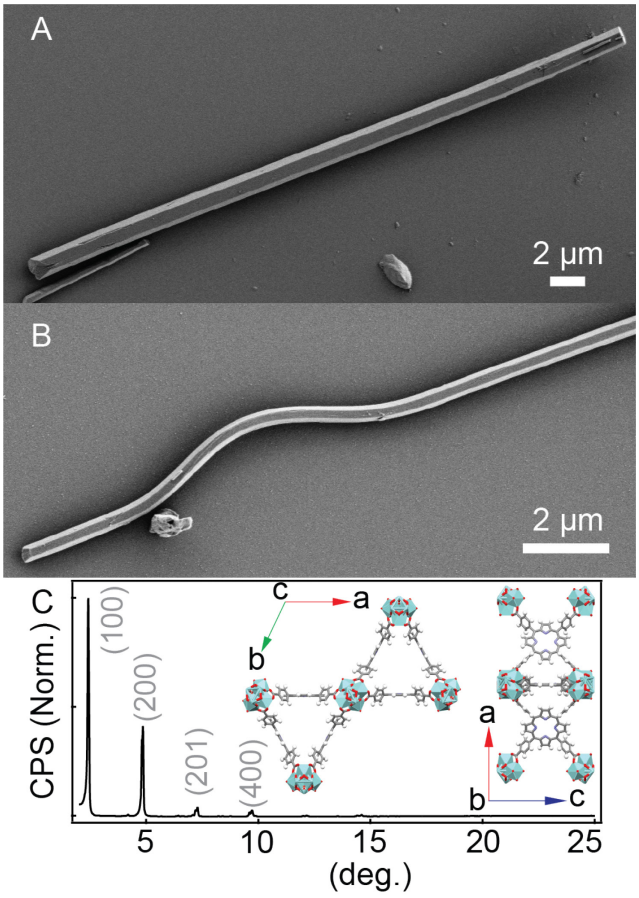

Figure 1. PCN-222 microrods. SEM images of a straight (A) and curved (B) rod. (C) Powder XRD pattern and crystal structure viewed along [001] and [010]. Pattern analysis shows a = 41.56 Å and c = 16.1 Å.

Figure 1, panels A and B, show representative scanning electron microscopy (SEM) images of straight and curved PCN-222 rods, respectively. The rods are faceted with hexagonal cross sections and, aside from the bend, show few structural defects visible on the surface. A survey of other SEM images (Fig. S1) shows that the hexagonal rods can bundle together forming more complex superstructures, and that the curved rods, which tend to be smaller in diameter, constitute approximately 10-20% of the total population. The powder XRD pattern of PCN-222 is shown in Fig. 1C, along with the crystal structure viewed along the [001] (left) and the [010] (right) direction, respectively.[19] The rods preferentially grow along the c axis, reaching 10 - 40 μm in length.

In Fig. 2A we show a PPM image of a typical PCN-222 rod, collected on a homebuilt pump-probe microscope (SI).[20] The transient transmission (ΔT) image is collected by scanning spatially overlapped pump (λ: 400 nm, $1/e^2$ width: 680 nm) and probe (800 nm) beams at a pump−probe delay time of Δt = 1 ps. The negative ΔT signal arises from a combination of Q-band absorption ($S_1 \rightarrow S_n$) and a photoinduced change in reflectivity.[21] For pulse energies up to 400 fJ (41 μJ/cm^2), decay kinetics (Fig. 2B) are power independent. At higher pump fluence, although the initial (Δt = 0 ps) signal size scales linearly with excitation power (Fig 2B. inset), nonlinear exciton-exciton annihilation processes begin to influence the decay kinetics. All subsequent data presented are collected with 300 fJ pulse energy to ensure that exciton-exciton interactions are negligible.[22]

That nonlinear decay kinetics are observed for relatively low excitation densities (~1.6×10^{18} cm^{-3}) suggests that excitons are mobile and frequently encounter other excitons, particularly at early times after photoexcitation. To quantify exciton transport, we turned to spatially separated PPM, in which the probe beam is positioned at a fixed location on a rod, and the pump beam is spatially scanned over the probe. Due to the narrow microrod width, we can only measure transport along the long (c-) axis. The resultant (1D) profiles (Fig. S5 and S6), collected at a series of pump-probe delay times, provide a direct probe of excited state transport in real space. For diffusive transport, the mean square deviation (MSD) of the profile increases linearly with delay time, Δt. As shown in Figs. 2C and 2D, excitons in the PCN-222 rods generally exhibit sub-diffusive transport, characterized by excitation profile MSDs that increase sub-linearly with time. Typically, such behavior is fit with a power law model, eq. 1.[23]

$$MSD(\Delta t) = A\Delta t^{\alpha} \quad (1)$$

Here A is a proportionality factor, and α is the diffusion exponent. For α = 1, Eq. 1 describes diffusive behavior, whereas α < 1 is characteristic of sub-diffusive transport. The time-dependent diffusion coefficient is proportional to the first derivative,

$$D_C(t) = \frac{1}{2}\alpha A t^{\alpha-1} \quad (2)$$

Figs. 2E and 2F respectively show histograms of α and the time-averaged diffusion constant $\langle D_c \rangle$, obtained by integrating Eq. 2 from Δt = 0 ps to 200 ps. 25 individual transport measurements on ten rods yield a mean α of 0.3 and $\langle D_c \rangle$ ranging between 0.27 and 1.0 cm^2/s.

Although direct transport measurements have not been previously reported for PCN-222, it is interesting to note that exciton diffusion constants (measured via PL quenching) for MOFs with comparable, aromatic linkers range between ~10^{-1} – 10^{-2} cm^2/s.[14, 24] The early time transport rates we measure for PCN-222 are larger than in these comparable systems and are larger than that predicted with Forster theory (SI), suggesting that non-thermalized transport[25], superradiance[12], or photon recycling[26] may influence exciton transport in this system. Further single particle studies will be important to understand the impact of these processes on energy transport and their interplay with structural defects.

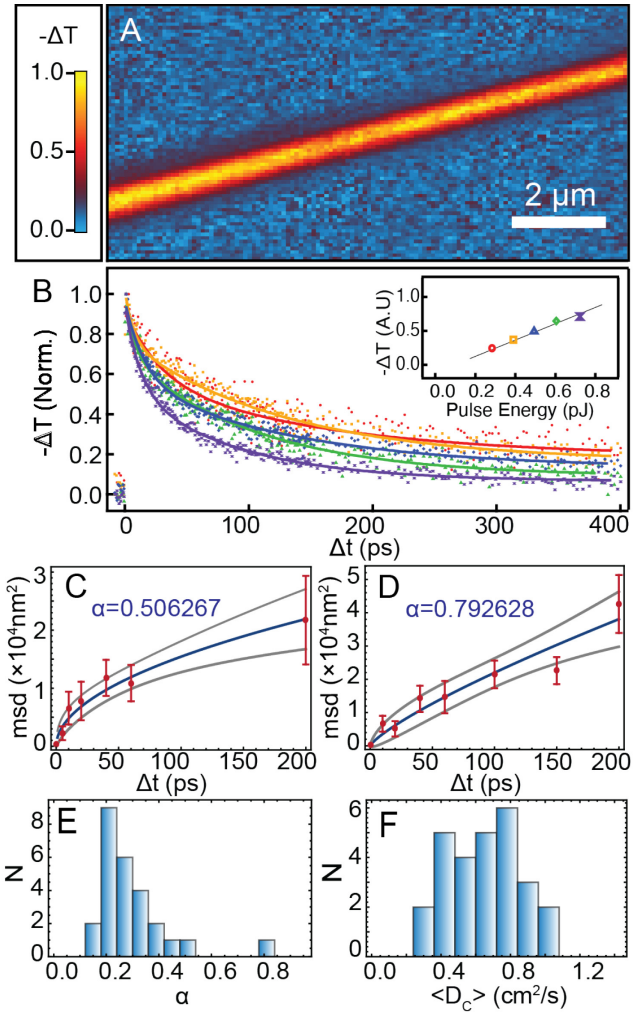

Figure 2. Power dependence and exciton transport in individual PCN-222 rods. (A) Pump-probe image of a single rod (B) Normalized power dependent decay kinetics. (C) and (D) show representative MSD vs. Δt for two PCN-222 rods. The blue line is a fit to Eq. 1 with 90% confidence intervals in gray. (E) and (F) Histogram showing distribution of α (see Eq. 1) and Δt-averaged diffusion constants.

At delay times greater than ~ 50 ps, transport slows down to rates more consistent with PL quenching measurements. Such sub-diffusive behavior is typically associated with energetic disorder, which causes exciton trapping at low energy sites. As trap sites are increasingly populated after photoexcitation, the population-averaged transport slows. We hypothesized that both sub-diffusive transport (Figs. 2C-E) and the overall distribution of $\langle D_c \rangle$ values we observed (Fig. 2F) reflect local energetic disorder, presumably a consequence of structural defects in the extended crystal.[27] To begin to address this hypothesis, we measured excited state decay kinetics for twelve PCN-222 microrods. Three representative datasets are shown in Figure 3. In general, we find that the kinetics collected from a single rod (over approximately 6 μm) are highly uniform. For example, each rod shows only a 15 ps variation in average relaxation lifetime (based on a triple exponential fit, see Table S1) measured between the 3 locations. On the other hand, when comparing kinetics between rods, the average decay lifetime of rods (i), (iii), and (ii) are 203 ps, 82 ps, and 61 ps, respectively.

The kinetic similarity observed over a short distance on a single rod, combined with the disparate kinetics observed between rods suggests that variation in defect density, likely in the form of linker or node vacancies, is responsible for the differences in excited state lifetime.[28] No correlation was found between excited-state lifetime and rod diameter (Fig. S4), suggesting that bulk defects, rather than surface states, are responsible for the difference in behavior. Variation in precursor or modulator concentrations, either spatially in the reaction vessel or over the growth period duration, is a likely cause of variable defect concentration.[10, 29]

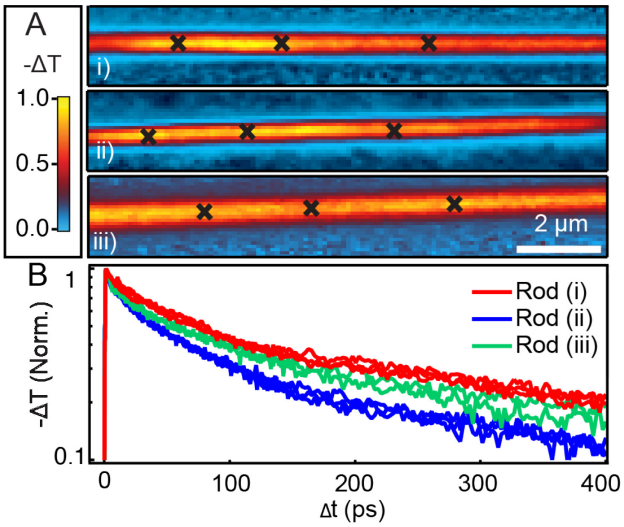

Figure 3. (A) Transient transmission images of rods (i), (ii), (iii). (B) Normalized kinetics collected from marked locations in panel (A).

Another indication of the impact of multi-scale structural defects can be observed when comparing the photophysical behavior of straight rods to those of bent rods (Figure 1A, B). Deposition of the rods on pre-stretched flexible substrates suggests the rods are brittle (Fig. S9). We, therefore, hypothesized that the observed bends are a direct manifestation of regions with high defect concentration – that is, the growth direction changes because defects accumulate in the crystal structure – and that distinct differences in photophysical behavior should be present in these regions.

To test this hypothesis, we compared both ΔT kinetics and PL quantum yield of straight and bent rods. Transient transmission images collected at Δt = 1 ps are shown in Figs. 4A and 4B, with high-resolution images of the boxed region shown in Figs. 4C and 4D. Although these images are normalized, the ΔT signal magnitude in the bent rod is comparable to that of any other straight rod on the substrate. The primary difference is in the relaxation kinetics: whereas the kinetics collected on the straight rod (Fig. 4G) are consistent with previous results (Fig. 3C), the curved rod kinetics (Fig. 4H) decay faster and exhibit significant variation of ~150 ps in average lifetime. We also collected steady-state photoluminescence images of the same region of each rod. The spectrally integrated PL images are shown in Figs. 4E and 4F, and while PL from the straight rod is clearly visible, PL from the bent rod is strongly quenched and difficult to distinguish from the background.

Without additional microscopic insight into both defect identity and their effect on the local and long-range electronic structure, it is difficult to know the precise origin of the difference in photophysical behavior. Nevertheless, the collection of results above suggests several important conclusions. First, it appears that exciton transport is exceptionally rapid in PCN-222, at least

in the first 10-100 ps after photoexcitation. Second, the presence of defects shortens both the excited state lifetime and the trasnport length. The nearly complete PL quenching in bent regions, where we expect defect density to be disproportionately high, suggests that defects facilitate non-radiative relaxation, perhaps in the form of a charge-transfer state or other low-energy trap with strong vibronic coupling to the ground state. Finally, because energy transport is efficient, defects are likely to have long-range impact on excited state dynamics, posing important challenges to light harvesting and other electronic and optoelectronic applications.

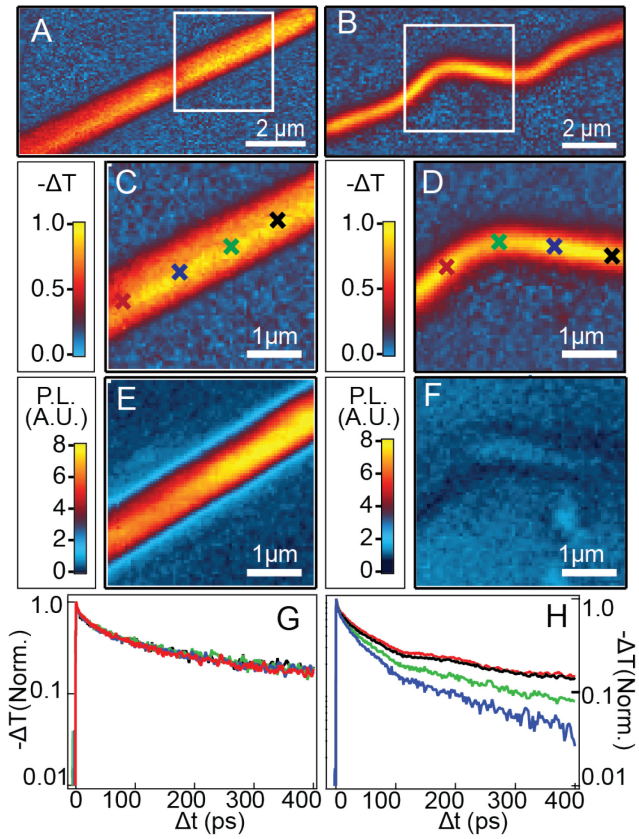

Figure 4. Spectroscopic comparison of straight and bent rods. (A) and (B) show transient transmission images of two rods. The boxed region in each is magnified in panels (C) and (D). Panels (E) and (F) show PL images of the straight and bent rods, respectively. (G) and (H) show transient transmission kinetics collected from the locations indicated in panels (C) and (D).

In conclusion, we have employed pump-probe and PL microscopy to investigate the excited state dynamics of single crystal PCN-222 microrods. The micron scale spectroscopic probes reveal exceptionally rapid exciton transport and important new insight into the effects of structural heterogeneity on excited state dynamics. These results highlight the importance of local spectroscopic probes to elucidate structure-function properties in MOF systems.

ASSOCIATED CONTENT

Supporting Information

Description of microscopy instrument and pump-probe measurements; Additional structural and spectroscopic data; Discussion of Förster energy transfer rate; Fit parameters for transient kinetics

AUTHOR INFORMATION

Corresponding Author

* erik.grumstrup@montana.edu
* ajmorris@vt.edu

ACKNOWLEDGMENT

S.A and E.M.G. supported by the National Science Foundation under Grant No. 2154448. X.Y and A.J.M. supported by the U.S. Department of Energy, Office of Science, Office of Basic Energy Sciences, under Award DE-SC0012445

ABBREVIATIONS

TCPP- Tetrakis (4-CarboxyPhenyl) Porphyrin; DFA- Difluoroacetic acid ; DMF- Dimethylformamide.

REFERENCES

(1) Rowsell, J. L. C.; Yaghi, O. M. Metal-organic frameworks: a new class of porous materials. *Micropor Mesopor Mat* **2004**, *73* (1-2), 3-14. DOI: 10.1016/j.micromeso.2004.03.034.

(2) Jiao, L.; Seow, J. Y. R.; Skinner, W. S.; Wang, Z. U.; Jiang, H. L. Metal-organic frameworks: Structures and functional applications. *Mater Today* **2019**, *27*, 43-68. DOI: 10.1016/j.mattod.2018.10.038.

(3) Hu, Z. J.; Meng, J.; Wang, X. M.; Li, W. T.; Chen, X. W. Tailoring the Surface Properties of Co-based Metal-Organic Frameworks for Highly Efficient and Selective Enrichment of Immunoglobulin G. *Acs Applied Materials & Interfaces* **2020**, *12* (49), 55453-55459. DOI: 10.1021/acsami.0c16821.

(4) Kim, D.; Liu, X. F.; Lah, M. S. Topology analysis of metal-organic frameworks based on metal-organic polyhedra as secondary or tertiary building units. *Inorg Chem Front* **2015**, *2* (4), 336-360. DOI: 10.1039/c4qi00236a.

(5) Long, J. R.; Yaghi, O. M. The pervasive chemistry of metal-organic frameworks. *Chem Soc Rev* **2009**, *38* (5), 1213-1214. DOI: 10.1039/b903811f. Zhou, H. C.; Long, J. R.; Yaghi, O. M. Introduction to Metal-Organic Frameworks. *Chem Rev* **2012**, *112* (2), 673-674. DOI: 10.1021/cr300014x. O'Keeffe, M.; Yaghi, O. M. Deconstructing the Crystal Structures of Metal-Organic Frameworks and Related Materials into Their Underlying Nets. *Chem Rev* **2012**, *112* (2), 675-702. DOI: 10.1021/cr200205j.

(6) Xu, H. Q.; Hu, J. H.; Wang, D. K.; Li, Z. H.; Zhang, Q.; Luo, Y.; Yu, S. H.; Jiang, H. L. Visible-Light Photoreduction of CO2 in a Metal-Organic Framework: Boosting Electron-Hole Separation via Electron Trap States. *J Am Chem Soc* **2015**, *137* (42), 13440-13443. DOI: 10.1021/jacs.5b08773.

(7) Lee, C. Y.; Farha, O. K.; Hong, B. J.; Sarjeant, A. A.; Nguyen, S. T.; Hupp, J. T. Light-Harvesting Metal-Organic Frameworks (MOFs): Efficient Strut-to-Strut Energy Transfer in Bodipy and Porphyrin-Based MOFs. *J Am Chem Soc* **2011**, *133* (40), 15858-15861. DOI: 10.1021/ja206029a.

(8) Shaikh, S. M.; Chakraborty, A.; Alatis, J.; Cai, M.; Danilov, E.; Morris, A. J. Light harvesting and energy transfer in a porphyrin-based metal organic framework. *Faraday Discussions* **2019**, *216*, 174-190. DOI: 10.1039/c8fd00194d.

(9) Schrimpf, W.; Ossato, G.; Hirschle, P.; Wuttke, S.; Lamb, D. C. Investigation of the Co-Dependence of Morphology and Fluorescence Lifetime in a Metal-Organic Framework. *Small* **2016**, *12* (27), 3651-3657. DOI: 10.1002/smll.201600619. Chen, X.; Jagadesan, P.; Valandro, S.; Hupp, J. T.; Schanze, K. S.; Goswami, S. Identifying the Polymorphs of Zr-Based Metal–Organic Frameworks via Time-Resolved Fluorescence Imaging. *ACS Materials Letters* **2022**, *4* (2), 370-377. DOI: 10.1021/acsmaterialslett.1c00754.

(10) Ameloot, R.; Vermoortele, F.; Hofkens, J.; De Schryver, F. C.; De Vos, D. E.; Roeffaers, M. B. Three-dimensional visualization of defects formed during the synthesis of metal-organic frameworks: a fluorescence microscopy study. *Angewandte Chemie* **2013**, *52* (1), 401-405. DOI: 10.1002/anie.201205627.

(11) Fang, Z. L.; Bueken, B.; De Vos, D. E.; Fischer, R. A. Defect-Engineered Metal-Organic Frameworks. *Angew Chem Int Edit* **2015**, *54* (25), 7234-7254. DOI: 10.1002/anie.201411540.

(12) Rajasree, S. S.; Yu, J.; Pratik, S. M.; Li, X.; Wang, R.; Kumbhar, A. S.; Goswami, S.; Cramer, C. J.; Deria, P. Superradiance and Directional Exciton Migration in Metal-Organic Frameworks. *Journal of the American Chemical Society* **2022**, *144* (3), 1396-1406. DOI: 10.1021/jacs.1c11979.

(13) Jin, S. Y.; Son, H. J.; Farha, O. K.; Wiederrecht, G. P.; Hupp, J. T. Energy Transfer from Quantum Dots to Metal-Organic Frameworks for Enhanced Light Harvesting. *J Am Chem Soc* **2013**, *135* (3), 955-958. DOI: 10.1021/ja3097114. Son, H. J.; Jin, S. Y.; Patwardhan, S.; Wezenberg, S. J.; Jeong, N. C.; So, M.; Wilmer, C. E.; Sarjeant, A. A.; Schatz, G. C.; Snurr, R. Q.; et al. Light-Harvesting and Ultrafast Energy Migration in Porphyrin-Based Metal-Organic Frameworks. *J Am Chem Soc* **2013**, *135* (2), 862-869. DOI: 10.1021/ja310596a. Deria, P.; Yu, J. R.; Balaraman, R. P.; Mashni, J.; White, S. N. Topology-dependent emissive properties of zirconium-based porphyrin MOFs. *Chem Commun* **2016**, *52* (88), 13031-13034. DOI: 10.1039/c6cc07343c. Rajasree, S. S.; Li, X. L.; Deria, P. Physical properties of porphyrin-based crystalline metal-organic frameworks. *Commun Chem* **2021**, *4* (1). DOI: 10.1038/s42004-021-00484-4. Goswami, S.; Chen, M.; Wasielewski, M. R.; Farha, O. K.; Hupp, J. T. Boosting Transport Distances for Molecular Excitons within Photoexcited Metal-Organic Framework Films. *Acs Applied Materials & Interfaces* **2018**, *10* (40), 34409-34417. DOI: 10.1021/acsami.8b14977.

(14) Gu, C.; Zhang, H.; Yu, J. H.; Shen, Q.; Luo, G. Q.; Chen, X.; Xue, P.; Wang, Z. B.; Hu, J. B. Assembled Exciton Dynamics in Porphyrin Metal-Organic Framework Nanofilms. *Nano Lett* **2021**, *21* (2), 1102-1107. DOI: 10.1021/acs.nanolett.0c04492.

(15) Skorupskii, G.; Le, K. N.; Cordova, D. L. M.; Yang, L. M.; Chen, T. Y.; Hendon, C. H.; Arguilla, M. Q.; Dinca, M. Porous lanthanide metal-organic frameworks with metallic conductivity. *P Natl Acad Sci USA* **2022**, *119* (34). DOI: 10.1073/pnas.2205127119. Dong, R.; Han, P.; Arora, H.; Ballabio, M.; Karakus, M.; Zhang, Z.; Shekhar, C.; Adler, P.; Petkov, P. S.; Erbe, A.; et al. High-mobility band-like charge transport in a semiconducting two-dimensional metal-organic framework. *Nat Mater* **2018**, *17* (11), 1027-1032. DOI: 10.1038/s41563-018-0189-z. Clough, A. J.; Skelton, J. M.; Downes, C. A.; de la Rosa, A. A.; Yoo, J. W.; Walsh, A.; Melot, B. C.; Marinescu, S. C. Metallic Conductivity in a Two-Dimensional Cobalt Dithiolene Metal–Organic Framework. *J Am Chem Soc* **2017**, *139* (31), 10863-10867. DOI: 10.1021/jacs.7b05742.

(16) Snider, J. L.; Su, J.; Verma, P.; El Gabaly, F.; Sugar, J. D.; Chen, L. N.; Chames, J. M.; Talin, A. A.; Dun, C. C.; Urban, J. J.; et al. Stabilized open metal sites in bimetallic metal-organic framework catalysts for hydrogen production from alcohols. *J Mater Chem A* **2021**, *9* (17), 10869-10881. DOI: 10.1039/d1ta00222h.

(17) Yang, X.; Bonnett, B. L.; Spiering, G. A.; Cornell, H. D.; Gibbons, B. J.; Moore, R. B.; Foster, E. J.; Morris, A. J. Understanding the Mechanical Reinforcement of Metal-Organic Framework-Polymer Composites: The Effect of Aspect Ratio. *ACS applied materials & interfaces* **2021**, *13* (44), 51894-51905. DOI: 10.1021/acsami.1c05430.

(18) Bonnett, B. L.; Smith, E. D.; De La Garza, M.; Cai, M.; Haag, J. V. I. V.; Serrano, J. M.; Cornell, H. D.; Gibbons, B.; Martin, S. M.; Morris, A. J. PCN-222 Metal–Organic Framework Nanoparticles with Tunable Pore Size for Nanocomposite Reverse Osmosis Membranes. *ACS Applied Materials & Interfaces* **2020**, *12* (13), 15765-15773. DOI: 10.1021/acsami.0c04349. Yang, X. Z.; Bonnett, B. L.; Spiering, G. A.; Cornell, H. D.; Gibbons, B. J.; Moore, R. B.; Foster, E. J.; Morris, A. J. Understanding the Mechanical Reinforcement of Metal-Organic Framework-Polymer Composites: The Effect of Aspect Ratio. *Acs Applied Materials & Interfaces* **2021**, *13* (44), 51894-51905. DOI: 10.1021/acsami.1c05430.

(19) Nazri, S.; Khajeh, M.; Oveisi, A. R.; Luque, R.; Rodriguez-Castellon, E.; Ghaffari-Moghaddam, M. Thiol-functionalized PCN-222 MOF for fast and selective extraction of gold ions from aqueous media. *Sep Purif Technol* **2021**, *259*. DOI: 10.1016/j.seppur.2020.118197. Feng, D. W.; Gu, Z. Y.; Li, J. R.; Jiang, H. L.; Wei, Z. W.; Zhou, H. C. Zirconium-Metalloporphyrin PCN-222: Mesoporous Metal-Organic Frameworks with Ultrahigh Stability as Biomimetic Catalysts. *Angew Chem Int Edit* **2012**, *51* (41), 10307-10310. DOI: 10.1002/anie.201204475.

(20) Hill, A. H.; Smyser, K. E.; Kennedy, C. L.; Massaro, E. S.; Grumstrup, E. M. Screened Charge Carrier Transport in Methylammonium Lead Iodide Perovskite Thin Films. *The Journal of Physical Chemistry Letters* **2017**, *8* (5), 948-953. DOI: 10.1021/acs.jpclett.7b00046.

(21) Mandal, A. K.; Taniguchi, M.; Diers, J. R.; Niedzwiedzki, D. M.; Kirmaier, C.; Lindsey, J. S.; Bocian, D. F.; Holten, D. Photophysical Properties and Electronic Structure of Porphyrins Bearing Zero to Four meso-Phenyl Substituents: New Insights into Seemingly Well Understood Tetrapyrroles. *J Phys Chem A* **2016**, *120* (49), 9719-9731. DOI: 10.1021/acs.jpca.6b09483.

(22) Grumstrup, E. M. Spatiotemporal coupling of excited state dynamics in time-resolved microscopies. *Opt Express* **2019**, *27* (22), 31385-31393. DOI: 10.1364/oe.27.031385.

(23) Akselrod, G. M.; Prins, F.; Poulikakos, L. V.; Lee, E. M. Y.; Weidman, M. C.; Mork, A. J.; Willard, A. P.; Bulovic, V.; Tisdale, W. A. Subdiffusive Exciton Transport in Quantum Dot Solids. *Nano Lett* **2014**, *14* (6), 3556-3562. DOI: 10.1021/nl501190s. Bouchaud, J. P.; Georges, A. Anomalous Diffusion in Disordered Media - Statistical Mechanisms, Models and Physical Applications. *Phys Rep* **1990**, *195* (4-5), 127-293. DOI: 10.1016/0370-1573(90)90099-N.

(24) Zhang, Q. Q.; Zhang, C. K.; Cao, L. Y.; Wang, Z.; An, B.; Lin, Z. K.; Huang, R. Y.; Zhang, Z. M.; Wang, C.; Lin, W. B. Forster Energy Transport in Metal-Organic Frameworks Is Beyond Step-by-Step Hopping. *J Am Chem Soc* **2016**, *138* (16), 5308-5315. DOI: 10.1021/jacs.6b01345.

(25) Deng, S.; Shi, E.; Yuan, L.; Jin, L.; Dou, L.; Huang, L. Long-range exciton transport and slow annihilation in two-dimensional hybrid perovskites. *Nature communications* **2020**, *11* (1), 664. DOI: 10.1038/s41467-020-14403-z. Pandya, R.; Chen, R. Y. S.; Gu, Q.; Gorman, J.; Auras, F.; Sung, J.; Friend, R.; Kukura, P.; Schnedermann, C.; Rao, A. Femtosecond Transient Absorption Microscopy of Singlet Exciton Motion in Side-Chain Engineered Perylene-Diimide Thin Films. *J Phys Chem A* **2020**, *124* (13), 2721-2730. DOI: 10.1021/acs.jpca.0c00346.

(26) Bercegol, A.; Ory, D.; Suchet, D.; Cacovich, S.; Fournier, O.; Rousset, J.; Lombez, L. Quantitative optical assessment of photonic and electronic properties in halide perovskite. *Nature communications* **2019**, *10* (1), 1586. DOI: 10.1038/s41467-019-09527-w. Diab, H.; Arnold, C.; Ledee, F.; Trippe-Allard, G.; Delport, G.; Vilar, C.; Bretenaker, F.; Barjon, J.; Lauret, J. S.; Deleporte, E.; et al. Impact of Reabsorption on the Emission Spectra and Recombination Dynamics of Hybrid Perovskite Single Crystals. *J Phys Chem Lett* **2017**, *8* (13), 2977-2983. DOI: 10.1021/acs.jpclett.7b00998.

(27) Shaikh, S. M.; Usov, P. M.; Zhu, J.; Cai, M.; Alatis, J.; Morris, A. J. Synthesis and Defect Characterization of Phase-Pure Zr-MOFs Based on Meso-tetracarboxyphenylporphyrin. *Inorg Chem* **2019**, *58* (8), 5145-5153. DOI: 10.1021/acs.inorgchem.9b00200.

(28) Sholl, D. S.; Lively, R. P. Defects in Metal-Organic Frameworks: Challenge or Opportunity? *J Phys Chem Lett* **2015**, *6* (17), 3437-3444. DOI: 10.1021/acs.jpclett.5b01135.

(29) Cai, W. X.; Lee, T.; Lee, M.; Cho, W.; Han, D. Y.; Choi, N.; Yip, A. C. K.; Choi, J. Thermal Structural Transitions and Carbon Dioxide Adsorption Properties of Zeolitic Imidazolate Framework-7 (ZIF-7). *J Am Chem Soc* **2014**, *136* (22), 7961-7971. DOI: 10.1021/ja5016298.

TOC Graphic